12th ANKARA INTERNATIONAL AEROSPACE CONFERENCE AIAC-2023-095
13-15 September 2023 - Online, Ankara TURKEY

THE INFLUENCE OF ATMOSPHERIC CONDITIONS ON AERODYNAMIC PERFORMANCE DEGRADATION IN AIRCRAFT ICING

Ömer Akbal[1]
Turkish Aerospace
Istanbul Technical University
Istanbul, Türkiye

Berkay Tetik[2]
Turkish Aerospace
Istanbul, Türkiye

Metin Orhan Kaya[3]
Istanbul Technical University
Istanbul, Türkiye

ABSTRACT

Icing can pose severe challenges to aircraft, leading to degradation in aerodynamic performance, increased weight, and a potential loss of control. Ensuring safe flight in icing environments requires thorough icing analyses during the design, certification, and requirement verification stages of air vehicles. This study focuses on the effects of ambient temperature and droplet diameter on ice accretion and aerodynamic degradation of the NACA 22112 airfoil. To achieve this objective, we employ the Response Surface Methodology (RSM), which proves to be an effective approach for modeling performance loss. In addition to uniform sampling data for atmospheric conditions, the study utilizes the Adaptive Sampling Method (ASM) to generate new samples and reduce the RSM error rate in terms of performance degradation. The findings of this study indicate that temperature and droplet diameter significantly influence the degradation of aerodynamic performance under the chosen FAR-25 Appendix-C icing conditions. Moreover, it is observed that considering icing types such as glaze, rime, and mixed is essential for establishing a comprehensive model between atmospheric conditions and aerodynamic performance degradation.

INTRODUCTION

Icing is a critical atmospheric phenomenon commonly encountered by air vehicles. The formation of ice on their surfaces can lead to significant issues, including decreased aerodynamic efficiency, increased flying weight, reduced stability, and even threats to flight safety. To ensure flight safety and implement effective measures for icing mitigation, thorough icing analyses are conducted throughout the design, certification, and requirement verification phases, considering relevant flight and atmospheric conditions.

Engineering problems are typically conducted under specific cost and time constraints. However, essential analyses and evaluations may vary and increase during the design and certification processes, resulting in higher labor and material costs. To address this challenge, the study employs an analytical technique to streamline the analysis and assess the sensitivity of inputs on the results. The study establishes an analysis matrix using atmospheric conditions, ambient temperature, and droplet diameter as inputs. Performance factors, such as lift and

[1] Turkish Aerospace, Istanbul Technical University, Email: omer.akbal@tai.com.tr, akbalom@itu.edu.tr
[2] Turkish Aerospace, Email: berkay.tetik2@tai.com.tr
[3] Istanbul Technical University, Email: kayam@itu.edu.tr

drag coefficients, along with the ice accumulation factor (ice weight), are then assessed to evaluate the influence of ice accretion.

There are numerous studies on the aforementioned subject available in the literature. For instance, Gray [1964] utilized an icing wind tunnel to investigate the effects of variables such as Liquid Water Content (LWC), Median Volume Diameter (MVD), ambient temperature, speed, angle of attack, and exposure time on ice accumulation shapes. However, the parameters considered in the study were insufficient for complete characterization, as they only accounted for ice formations in terms of horn length and angle, neglecting lift and moment coefficients in the aerodynamic criterion [Gray, V. H., 2009].

Similarly, Shin et al. [1992] numerically studied the effect of free-stream velocity and ambient temperature on ice shapes. They observed that the loss of aerodynamic performance caused by glaze ice at higher temperatures was greater than that caused by rime ice at lower temperatures. Nevertheless, the number of cases analyzed in the study was inadequate to establish a reliable relationship. Additionally, when comparing the numerical results to experimental data, reasonable agreement was found for rime ice, but significant variances were observed for glaze ice [Shin, J., and Bond, T. H., 1992].

Son et al. [2013] employed RSM to assess the correlation in their study, which examined the performance deterioration of iced airfoils utilizing the conditions specified in the FAR-25 Appendix C envelope for intermittent flying. In conclusion, they demonstrated that the lift and drag coefficients were significantly affected at an ambient temperature of -10 °C and LWC values greater than 2 g/m^3. Moreover, the moment coefficient was intensely lowered at temperatures below -40 °C and with high MVD values. Notably, they found that the effect of exposure time on performance degradation was negligible within the limitations specified in their paper [Son, C., Yee, K., and Oh, S., 2013].

According to the literature [Fajt, Hann, and Lutz, 2019], conducting large parametric studies on meteorological conditions is essential to investigate the aerodynamic performance degradation of Unmanned Aerial Vehicles (UAVs) under a wide variety of icing scenarios. Considering meteorological impacts is critical for developing effective ice protection strategies. In this study, FENSAP-ICE was employed to perform numerical Computational Fluid Dynamics (CFD) simulations of ice accretion and assess the performance of a 2D airfoil.

In this study, RSM is utilized to model aerodynamic performance degradation under atmospheric conditions defined in FAR-25 Appendix-C. RSM is a statistical method that estimates data based on experimental relationships between independent variables (inputs) and known outputs (responses). It has gained popularity due to its ability to provide meaningful and reliable information while using fewer computational resources [Colaco, M.J., and Dulikravich, G.S., 2011]. For instance, Phan et al. [2019] presented a study on CFD-based response surface methodology for thermal simulation and optimization of data centers.

Moreover, initial icing analyses were conducted through uniform sampling of the Appendix-C envelope for the NACA 22112 airfoil. Based on the results, the analysis matrix was expanded by identifying points where the analyses should be concentrated using adaptive sampling (Bayesian optimization). This approach is expected to reduce the average error rate of the response surface expression, enabling the evaluation of the effect of flight conditions on icing severity and aerodynamic efficiency with minimal analysis while achieving a low error rate.

METHOD

Numerical Method

Ice accretion analyses are conducted using ANSYS FENSAP-ICE 2022 R2 commercial software with the multi-shot method. Firstly, flow field solutions are computed with the FENSAP module to obtain velocity and pressure distributions. Using the Eulerian equations, the velocity of a droplet is then calculated in the discrete domain, where the airflow variables are known. After that, computations are performed for heat transfer coefficients on the surface, energy balance, and ice accumulation. Subsequently, a new iced geometry is generated for the following time step based on the ice thickness determined by shear stress and heat flux

distribution. This procedure is repeated at specified intervals throughout the icing period, and it is referred to as the multi-shot analysis, as illustrated in Figure 1.

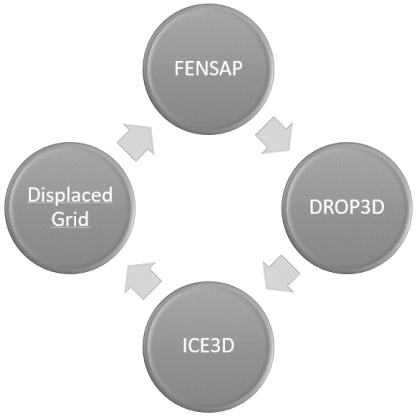

Figure 1: Multi-shot ice accretion stages

Validation

The validation of ice accretion prediction is based on experimental data for a horn ice case of the NACA-23012 airfoil, as published in [Broeren, A.P., Addy, H.E., 2011]. The simulations are performed using the k-ω SST turbulence model. An overview of the experimental icing case and its corresponding parameters is provided in Table 1. These parameters include chord length, LWC, MVD, cruising speed, ambient temperature, AoA, and icing exposure time.

Chord	0.4572 m
Liquid Water Content	0.75 $g\ m^{-3}$
Median Volumetric	15.4 μm
Velocity	102.88 ms^{-1}
Static Temperature	-7.5 °C
Angle of Attack	2
Exposure Time	300 s

Table 1*:* Icing conditions for validation test case

The initial step of the ice accretion analysis is to predict flow field parameters. To achieve this, velocity and pressure distributions are determined to calculate droplet trajectories and later collection efficiencies. The last step involves predicting ice shapes on the airfoil using accretion models. Since single-layer ice accretion analyses may be inaccurate, a multi-shot approach is used to achieve more accurate predictions. The FENSAP-ICE tool includes various modules with different purposes, and it serves as a state-of-the-art CFD solver that obtains the airflow solution by solving compressible Reynolds-averaged Navier-Stokes equations. In the multi-shot approach, grid deformation is required when ice grows on the airfoil surface. Fluent meshing is utilized for this re-meshing process. Consequently, the icing exposure time is divided into smaller steady-state intervals. Based on the results, the ice accretion process is divided into eight shots. Figure 2 depicts the predicted and experimental ice shapes.

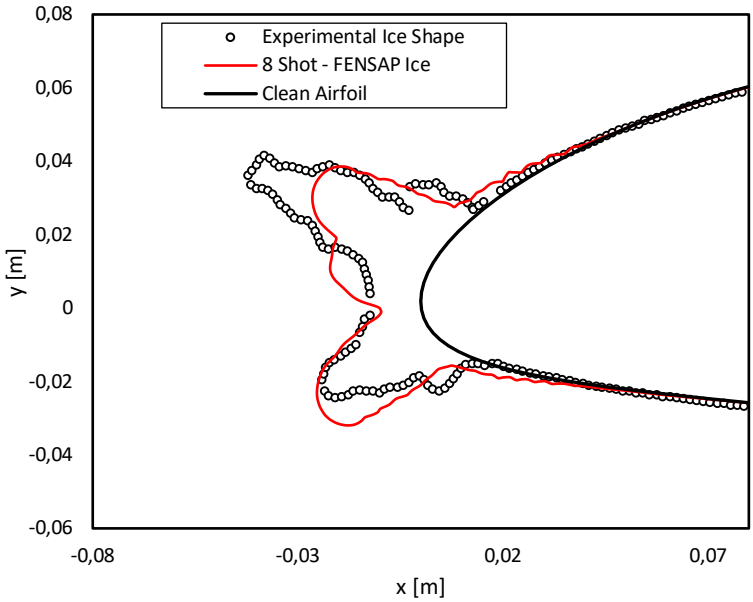

Figure 2: Validation of ice shape result vs experimental result

Afterwards, CFD analyses were conducted for both clean and iced airfoils using ANSYS Fluent 2022 R2, with the Transition-SST turbulence model employed in these analyses. To accurately model the ice formation, k/c = 0.0026 roughness was applied to the leading edge, where "k" represents the ice roughness height and "c" denotes the chord length. Figure 3 illustrates the good agreement between the numerical and experimental results.

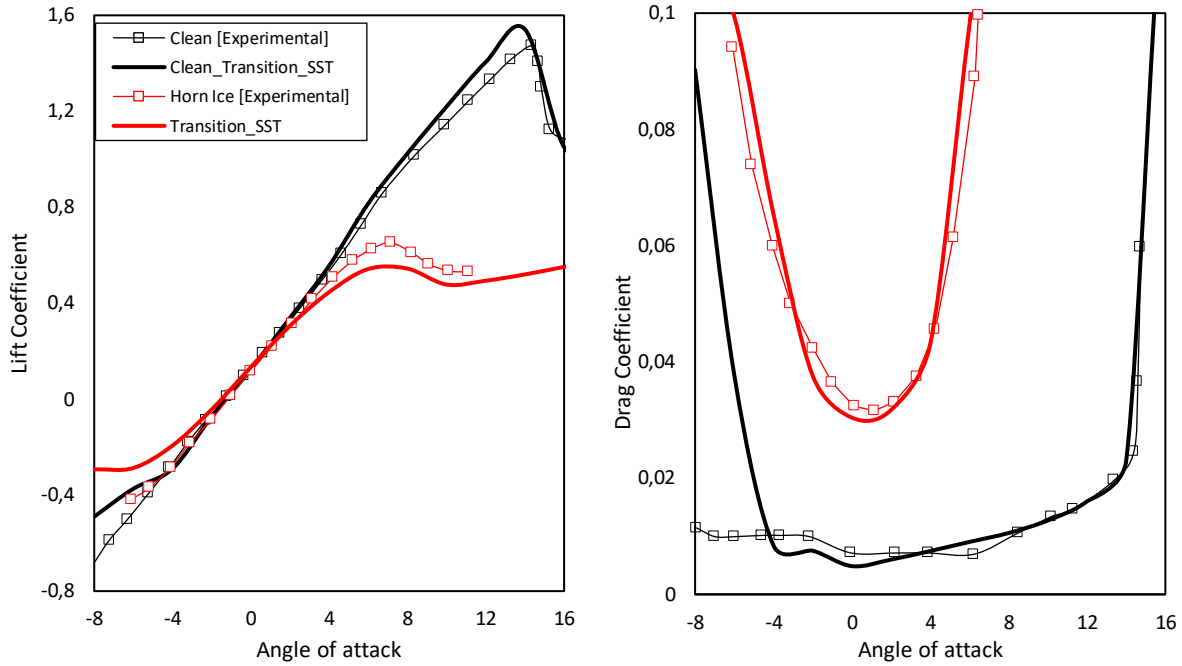

Figure 3: c_L – c_D curves of NACA-23012 airfoil; numerical vs experimental result

Methods Specific to the Study (DOE)

Adaptive Sampling: In this study, Adaptive Sampling, a sequential design method, was applied with Bayesian Optimization as part of the Design of Experiments. Bayesian Optimization is an iterative method used for modeling black-box functions, especially in situations where the objective function is complex and lacks a closed form, no gradient information is available, and function evaluations are expensive. The procedure essentially

consists of the following steps, as defined in the reference [Zhang, Y., Neelakantan, A., Park, C., Kim, N.H., Lam, H., Haftka, R.T., 2019]:

1) Choose a surrogate model for modeling the true function f and define its prior.
2) Given the set of outputs, use Bayes rule to obtain the posterior
3) Use an acquisition function $\alpha(x)$, which is a function of posterior, to decide the next sample point as shown in equation 1.

$$x_t = \mathrm{argmax}_x \alpha(x) \quad (1)$$

4) Add newly sampled data to set of outputs and go to step 2 till convergence.

Thus, new samples are obtained in areas with higher gradients, which are more difficult to predict via adaptive sampling.

Response Surface Method: To develop a response model for calculating data points in conjunction with experimental or numerical analysis theories, response surface modeling is employed. The generic form of the relationship is as follows [Myers, R.H., Montgomery, D.C., 1995]:

$$y = F(x_1, x_2, \dots, x_3) + \varepsilon \quad (2)$$

In the equation, y represents the response variable, x_i denotes the design variables, and ε is the total error, assumed to follow a normal distribution with a zero mean. The response surface model F is typically considered a quadratic polynomial. The response factors, namely ice weight, lift, and drag coefficients, were determined, while the design variables were identified as ambient temperature and droplet diameter. Detailed boundary conditions are provided in the icing scenarios section. Figure 4 illustrates the RSM modeling for a sample dataset.

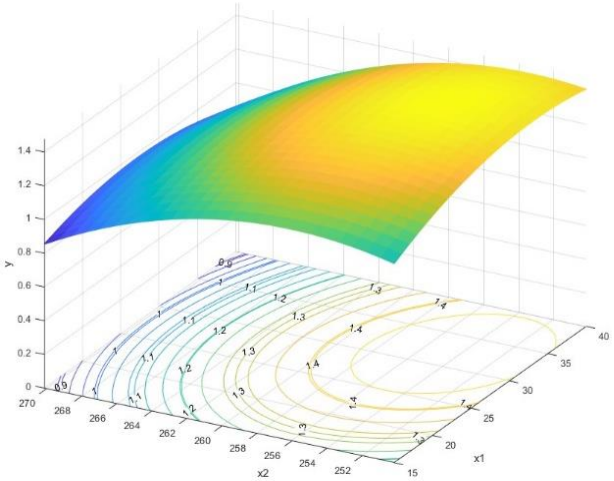

Figure 4: The illustration of RSM modeling for a sample dataset

ICING SCENARIOS

Uniform Sampling Analysis

In this study, the flight scenario was defined as a 17.6 nm horizontal flight for 300 seconds at an altitude of 15,000 ft, utilizing the NACA-22112 airfoil profile, a 4° angle of attack, and an airspeed of 109 m/s. Meteorological conditions corresponding to the limits of maximum continuous icing, as outlined in the FAR-25 Appendix-C chart, were selected and are presented in Figure 5. LWC values were obtained as a function of changing ambient temperature and droplet diameter. To investigate the effects of varying icing conditions on aerodynamic performance, a total of 30 different icing scenarios were evaluated as inputs for the Adaptive Sampling and RSM analyses.

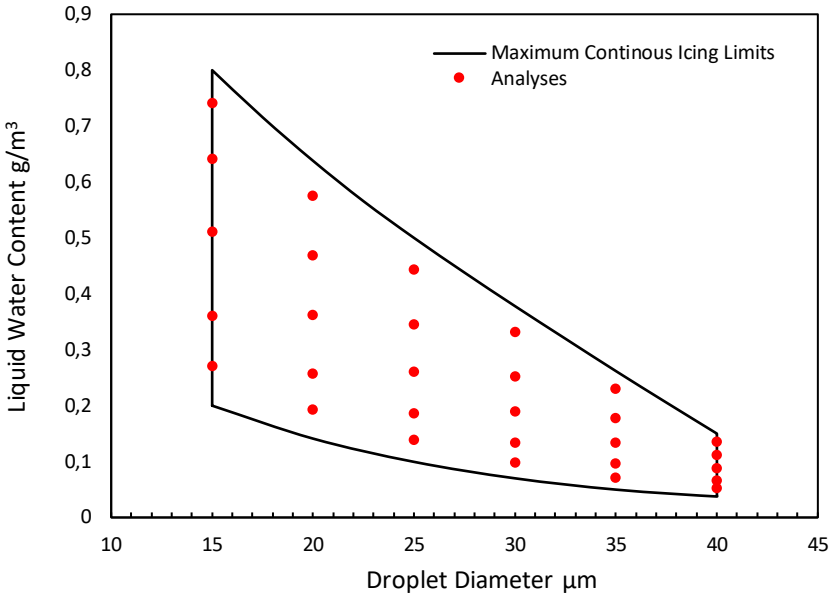

Figure 5: Analysis points (Maximum continuous condition in FAR-25 Appendix-C)

Adaptive Sampling Method

For the NACA-22112 airfoil with a chord length of 0.4572 m, a total of 30 ice accumulation analyses were performed for the preliminary analysis at a 4° angle of attack, 109 m/s air velocity, and a constant altitude condition. Ice accumulation analyses were carried out on 6 different droplet diameters and 5 different temperature values and were performed with 10 shots, each for 30 seconds, using the multi-shot method. The conditions are tabulated in Table 2. The ice area of each ice accumulation and the corresponding ice mass were calculated.

Velocity (m/s)	109
$\mathbf{T}_\infty$ (K)	[250.15 270.15]
Angle of Attack	4°
MVD (µm)	[15 40]
Exposure Time (sn)	30×10
Turbulence Model	k-ω SST
T_{wall} (K)	T_0 + 10
Droplet Distribution	Monodisperse
Ice Density	Constant

Table 2: Icing analysis conditions and setup

Furthermore, the lift and drag coefficients of each ice shape were calculated at different AoA, ranging from -6° to 15°, using ANSYS Fluent 2022 R2. In the flow analysis, the static temperature (T_∞) is 258.35 K, and the Reynolds number is 2.34 million. The ice formations that occurred under the specified conditions and the corresponding c_L and c_D curves are presented in Figures 6-8.

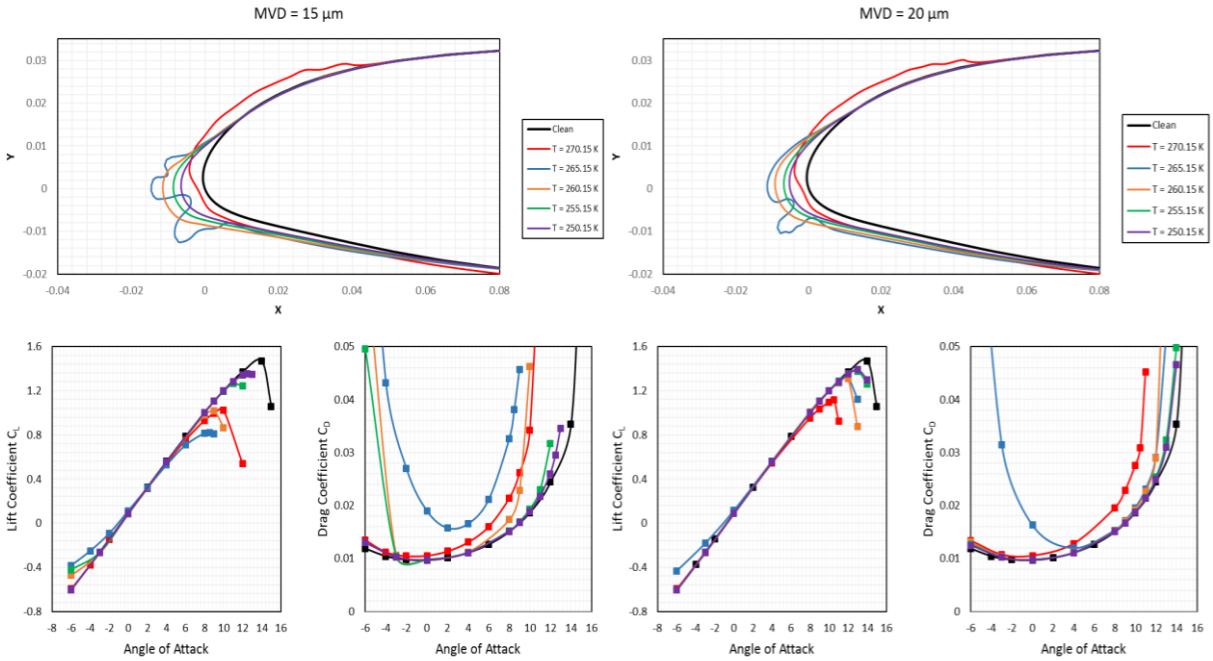

Figure 6: Ice formations and c_L – c_D curves for 15 µm MVD (left) and 20 µm MVD (right)

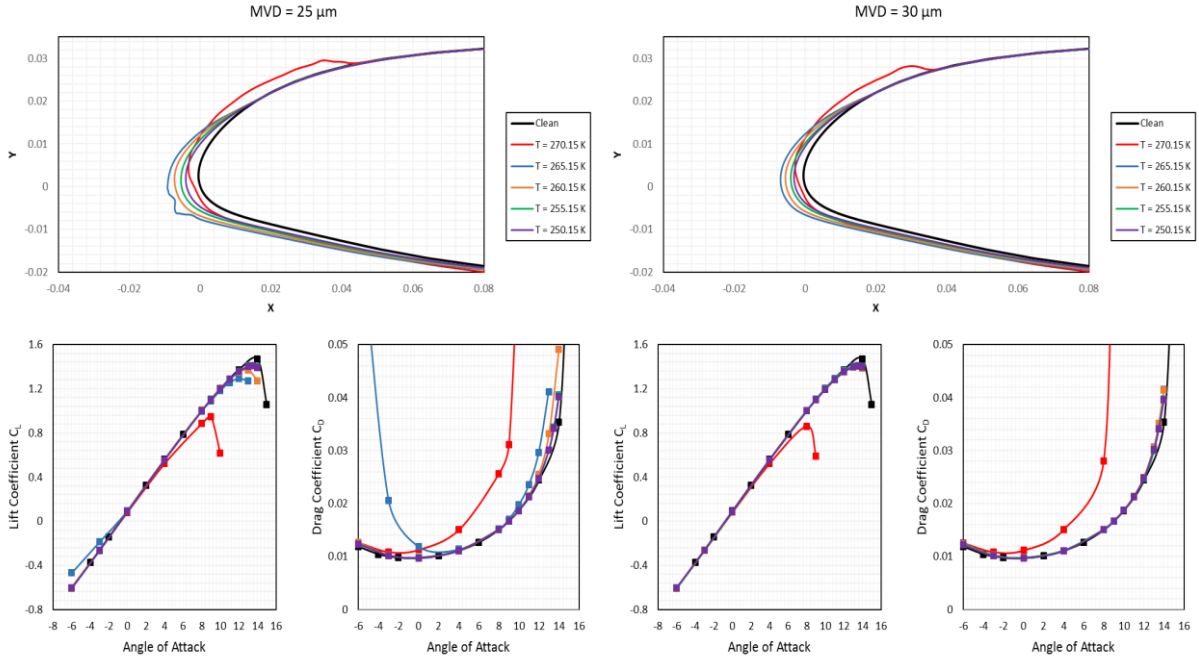

Figure 7: Ice formations and c_L – c_D curves for 25 µm MVD (left) and 30 µm MVD (right)

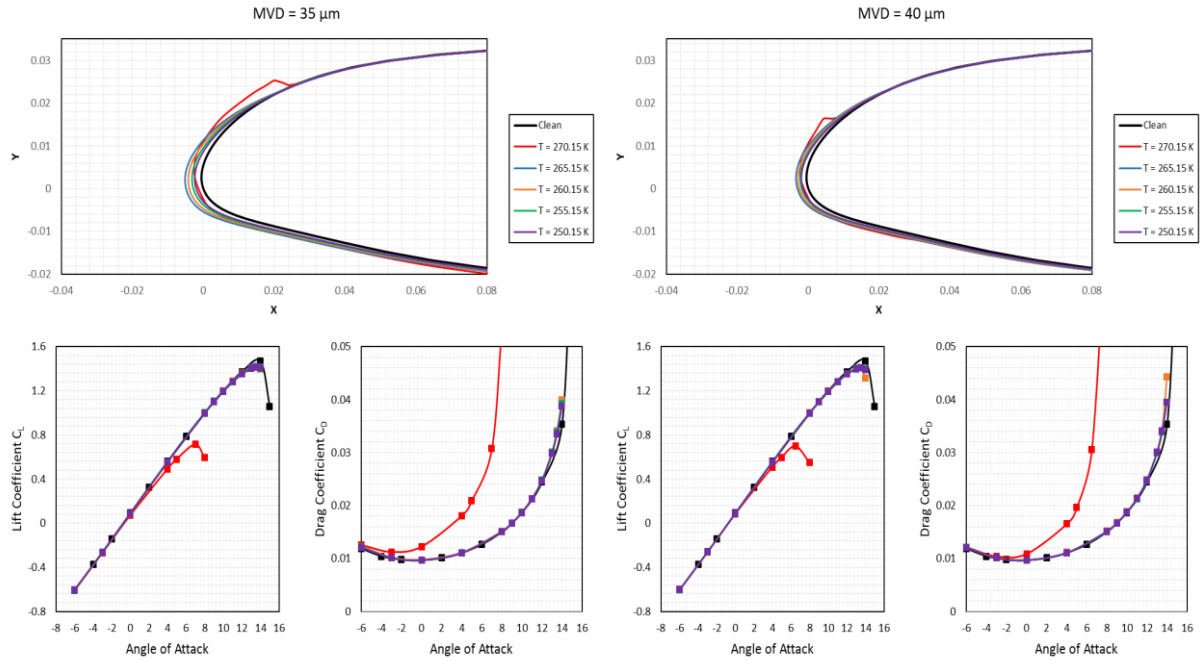

Figure 8*:* Ice formations and c_L – c_D curves for 35 µm MVD (left) and 40 µm MVD (right)

To establish a reliable correlation for unsolved conditions, we employed the response surface regression model to investigate the impacts of flight and atmospheric conditions on icing and, consequently, on aerodynamic performance loss. The model's design variables included the maximum lift coefficient and aerodynamic efficiency (c_L/c_D) values at a 4° AoA, representing aerodynamic degradation, and the ice mass, accounting for variations in flight weight. The average error rates between the model's predicted responses and the actual values were 8.86 % for $\mathbf{c_{l,max}}$, 6.48 % for c_L/c_D, and 11.63 % for ice mass. As a result, the response surface regression model allows obtaining responses within specified error limits for any condition without a known condition. Figure 9 shows the response surfaces between aerodynamic performance degradation and meteorological conditions. Additionally, Figure 10 presents the ice mass contour.

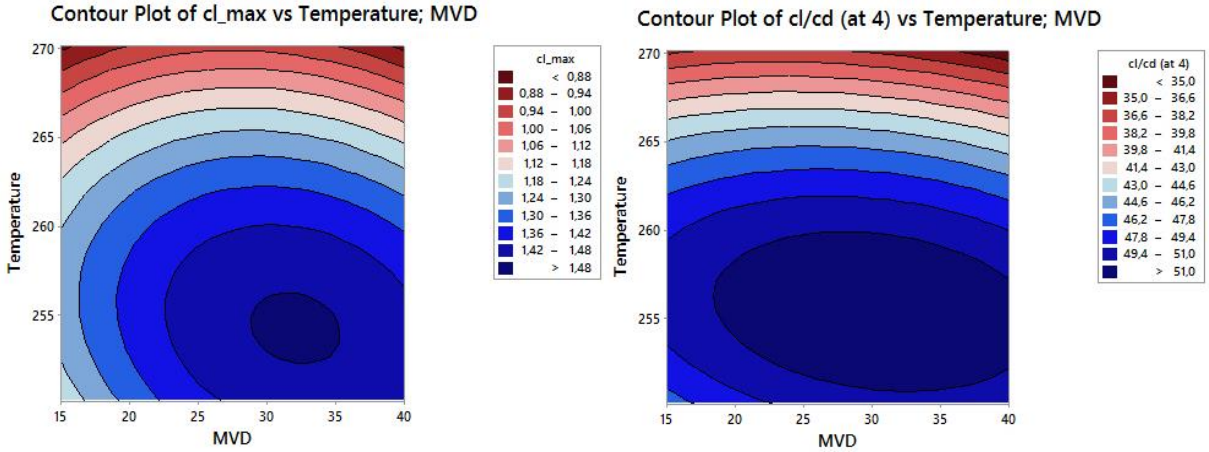

Figure 9*:* $c_{l,max}$ (left) $(c_l/c_d)_{4°}$ (right) values according to regression equation

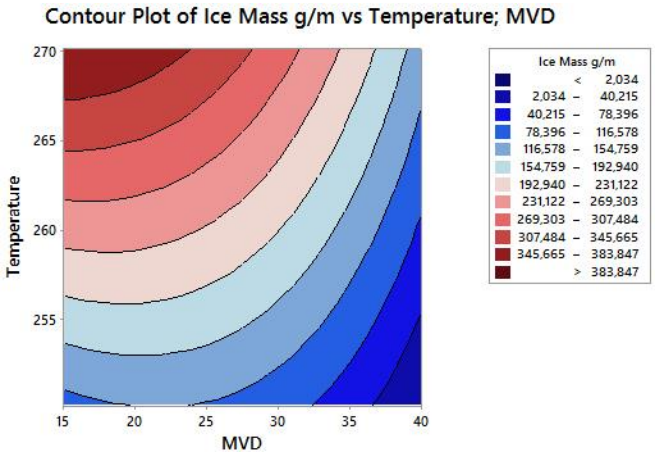

Figure 10*:* Ice mass values according to regression equation

The R^2 parameter used to evaluate the performance of the regression model is 69.84% for $c_{l,max}$, 69.04% for aerodynamic efficiency at 4°, and 96.9% for ice mass. Thus, the sensitivity and effect of droplet diameter and static temperature on amount of icing and aerodynamic degradation for the NACA-22112 airfoil were determined. On the other hand, it may be possible to reduce the error rates and establish a more sensitive correlation by increasing the amount of analysis and defining the ice formations in more detail. For this reason, adaptive sampling method was applied on the available conditions and results, so that the sensitive regions in the solution space where the variation was high were determined and the sample was expanded. BoTorch, a Python library built on GPyTorch and Ax, was used for adaptive sampling in the study. The code applies Bayesian optimization to explore the black-box function (the hypothetical expression that describes the relationship between inputs and outputs). On the other hand, the "expected improvement (EI)" method was used as the acquisition function in optimization. In the method, the function f is evaluated at the point that most improves f' in expectation.

$$u(x) = max(0, f' - f(x)) \tag{3}$$

The EI acquisition function is the expected utility as a function of $\boldsymbol{x}$, and ultimately the point with the highest expected improvement is selected. While expanding the analysis matrix, a severity parameter including $\mathbf{c_{l,max}}$, c_L/c_D and ice mass values has been fitted for a more holistic approach. The calculation of the parameter is as in Equation 4.

$$S_i = \frac{1}{5}\left[2\left(1 - \frac{c_{l,max,i} - \min(c_{l,max})}{\max(c_{l,max}) - \min(c_{l,max})}\right) + 2\left(1 - \frac{(c_l/c_d)_{4°,i} - \min((c_l/c_d)_{4°})}{\max((c_l/c_d)_{4°}) - \min((c_l/c_d)_{4°})}\right) + \left(\frac{m_{ice,i} - \min(m_{ice})}{\max(m_{ice}) - \min(m_{ice})}\right)\right] \tag{4}$$

At the preliminary analysis points chosen using uniform sampling, the outcomes and severity values are as shown in Table 3.

Case No	$c_{l,max}$	c_l/c_d (at 4°)	Ice Mass (g/m)	Severity Index
1	1.0228	41.415	343.6	0.5457
2	0.8218	31.788	290.9	0.7946
3	1.0162	49.438	256.3	0.3628
4	1.2668	50.151	175.5	0.1674
5	1.3533	50.114	123.5	0.0916
6	1.1172	42.519	393.1	0.5014
7	1.3128	46.735	339.0	0.2906
8	1.3084	50.131	255.8	0.1887
9	1.3778	50.174	173.1	0.1042
10	1.3899	50.162	125.2	0.0714
11	0.9441	34.756	349.3	0.7075
12	1.2911	48.904	319.4	0.2543
13	1.3705	50.268	226.6	0.1359
14	1.4093	50.126	154.0	0.0771
15	1.4085	50.239	106.4	0.0495
16	0.8595	34.574	297.6	0.7292
17	1.4058	50.133	247.2	0.1300
18	1.4017	50.103	185.1	0.0987
19	1.4052	50.153	120.6	0.0606
20	1.4065	50.110	80.4	0.0386
21	0.7139	27.129	214.2	0.8929
22	1.4195	50.201	184.3	0.0868
23	1.4114	50.162	136.7	0.0658
24	1.4125	50.161	85.7	0.0373
25	1.4120	50.222	51.6	0.0179
26	0.6975	30.835	111.7	0.7818
27	1.4096	50.156	114.7	0.0549
28	1.4098	49.990	81.8	0.0397
29	1.4083	50.112	51.6	0.0218
30	1.4061	50.083	28.1	0.0106

Table 3: Results of preliminary analyses

In Figure 11, we present the new analysis points obtained using the adaptive sampling technique as a DOE strategy. The figure illustrates the icing severity index for aerodynamic performance loss. It is observed that new samples for icing conditions have been generated where the index gradient is high. This evaluation suggests that the near-freezing temperature is a critical factor contributing to performance loss. Table 4 provides a tabulation of additional sample conditions after the adaptive sampling method.

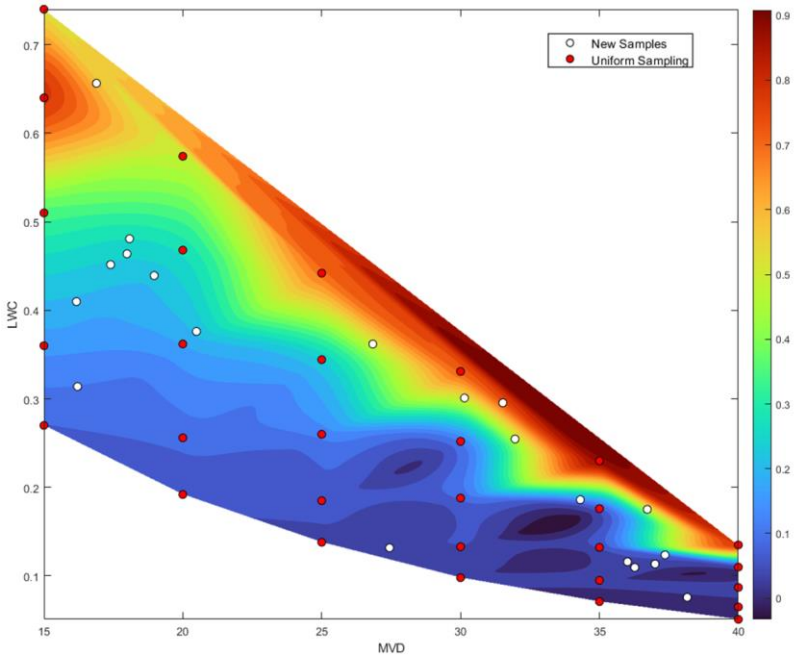

Figure 11: Severity contour and new samples obtained by adaptive sampling

Sample No	MVD	T (K)	LWC
1	37.00	260.23	0.1135
2	16.21	254.51	0.3139
3	36.01	259.24	0.1160
4	16.17	257.95	0.4098
5	17.40	260.87	0.4516
6	17.99	262.06	0.4638
7	18.97	262.34	0.4392
8	18.08	262.87	0.4808
9	36.27	258.63	0.1096
10	26.84	268.13	0.3619
11	36.72	267.74	0.1752
12	27.44	253.18	0.1318
13	30.14	268.42	0.3010
14	31.52	269.85	0.2955
15	37.36	262.45	0.1237
16	34.31	265.17	0.1861
17	31.96	267.52	0.2546
18	38.16	255.22	0.0758
19	16.89	269.36	0.6564
20	20.49	261.39	0.3761

Table 4: Atmospheric conditions of new samples

Results

Ice accumulation analyses were conducted for the new analysis conditions acquired through the adaptive sampling approach, and aerodynamic coefficients were computed for the resulting iced geometries. The obtained outcomes for the four most critical icing conditions are depicted in Figure 12.

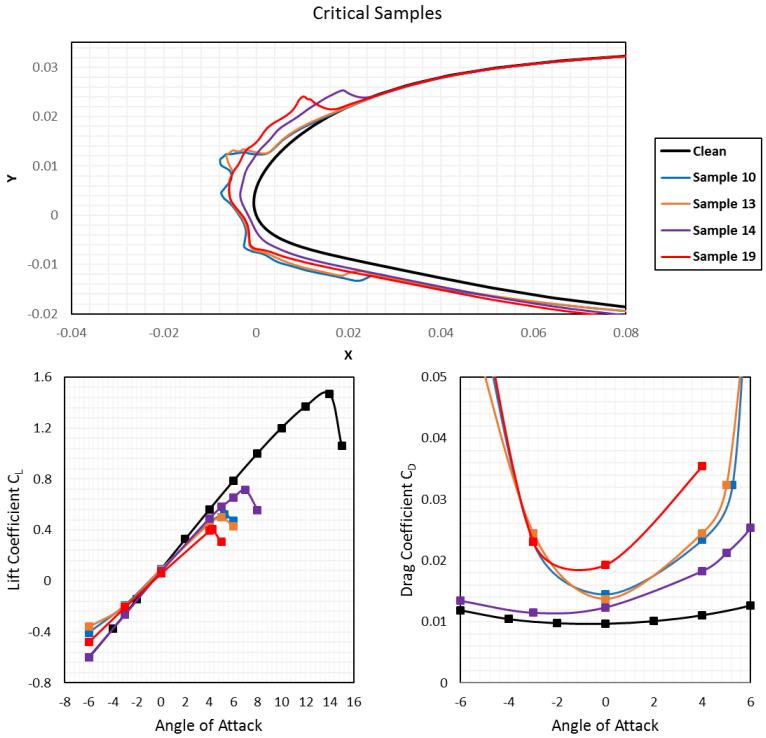

Figure 12: Ice formations and c_l - c_d curves of most critical samples

In critical cases, it was observed that ice accumulation, which took place when the ambient temperature was slightly below freezing, led to a transformation of the airfoil into a blunt structure, resulting in the most significant aerodynamic degradation under these conditions. Figure 13 illustrates flow separation occurring from the top of the ice formation, as evidenced by the velocity distribution contour of Sample 19 at a 4.5° angle of attack. Due to this phenomenon, the stall angle decreases significantly under critical icing conditions.

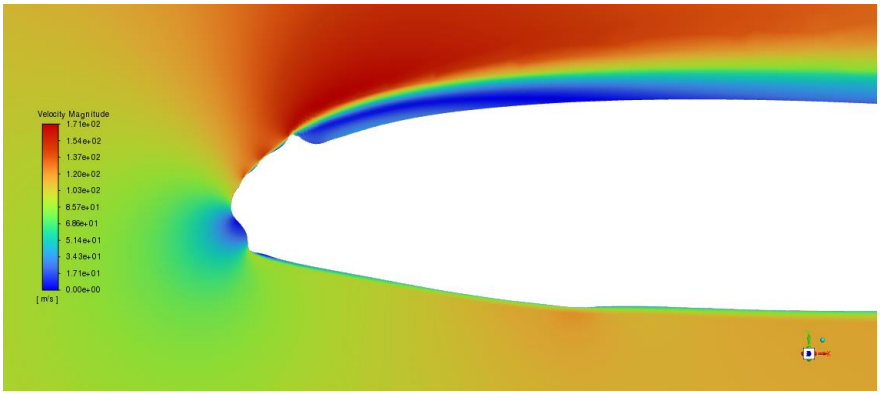

Figure 13: Velocity magnitude contour of sample 19 (at 4.5°)

Furthermore, the response surface regression model was reapplied to an expanded sample, and the resultant changes were examined. In the new regression equations obtained, the R^2 parameter is 63.18% for $c_{l,max}$, 56.9% for aerodynamic efficiency at 4°, and 97.59% for ice mass. On the other hand, the average error rate of the model is 18.91% for $c_{l,max}$, 14.84% for c_l/c_d, and 8.26% for ice mass. Especially with the high LWC value and the transformation of ice formations to glaze ice type at temperatures close to the freezing temperature, the deviation in the regression model increased even more. Considering the entire condition space, the region corresponding to glaze-type icing covers a narrow temperature range, and the regression equations are expressed in a quadratic polynomial form, making it challenging to achieve an expression with a low error rate. The resulting RSM contours for the design variables are depicted in Figure 14 and 15.

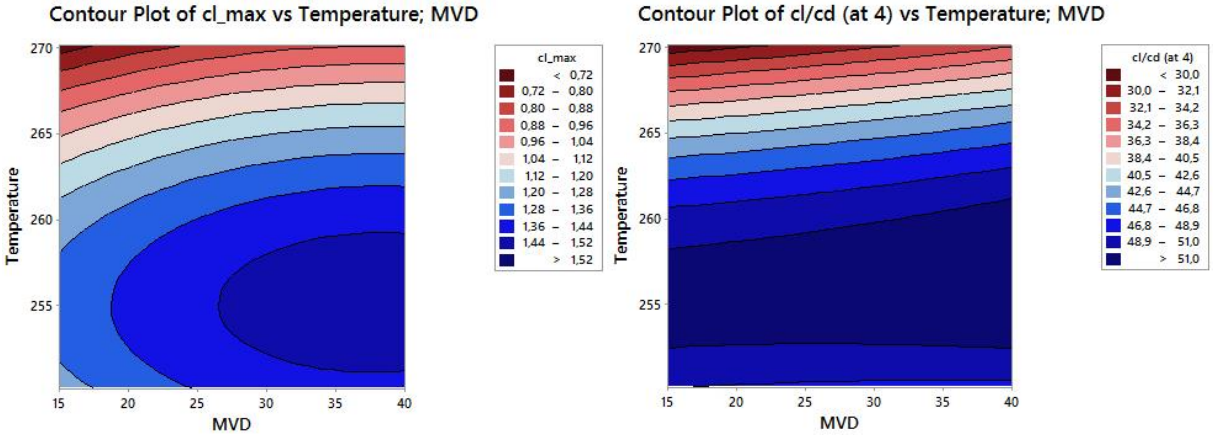

Figure 14: $c_{l,max}$ (left) $(c_l/c_d)_{4^\circ}$ (right) values according to regression equation of all analyzes

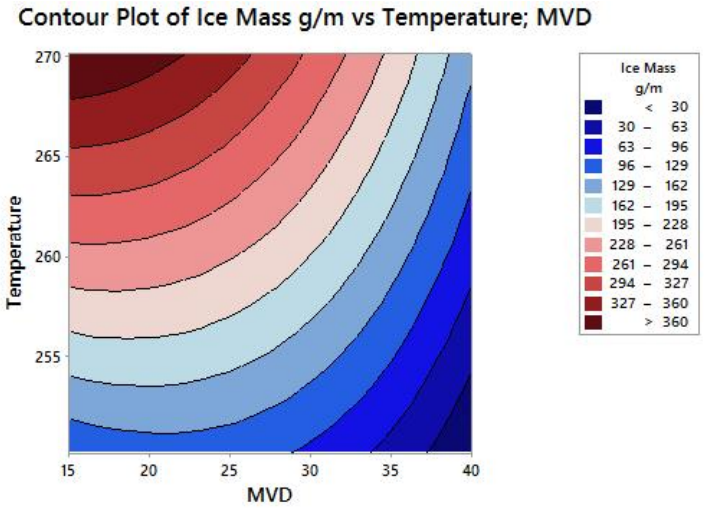

Figure 15*:* Ice mass values according to regression equation of all analyzes

The expressions obtained through the regression model, namely, equations 5, 6, and 7, are presented below, where X represents the MVD value, and Y represents the ambient temperature in Kelvin (K) within the equations.

$$c_{l,max} = -173.8 + 0.011X + 1.372Y - 0.000334X^2 - 0.002693Y^2 + 0.000058XY \quad (5)$$

$$(c_l/c_d)_{4^\circ} = -6867 - 3.13X + 54.4Y + 0.0012X^2 - 0.1068Y^2 + 0.0121XY \quad (6)$$

$$m_{ice} = -9355 + 88.7\,X + 54.3Y - 0.3346\,X^2 - 0.0681Y^2 - 0.2977XY \quad (7)$$

Table 5 and 6 present the CFD results, $c_{l,max}$, $(c_l/c_d)_{4^\circ}$, and m_{ice} values, obtained using the regression equation for all analysis conditions. Generally, the aerodynamic coefficient's error rate is notably higher in temperatures close to freezing, allowing glaze-type icing. However, this correlation is not significant as the ice mass is primarily associated with the LWC value.

Case	MVD	T_∞ (K)	Fluent Results			Regression Model		
			$c_{l,max}$	$(c_l/c_d)_{4^\circ}$	m_{ice}	$c_{l,max}$	$(c_l/c_d)_{4^\circ}$	m_{ice}
1	15	270.15	1.0228	41.415	343.6	0.6824	28.554	390.2
2	15	265.15	0.8218	31.788	290.9	1.0254	41.677	323.3
3	15	260.15	1.0162	49.438	256.3	1.2339	49.459	253.0
4	15	255.15	1.2668	50.151	175.5	1.3076	51.901	179.2
5	15	250.15	1.3533	50.114	123.5	1.2467	49.002	102.1
6	20	270.15	1.1172	42.519	393.1	0.7552	29.513	373.1
7	20	265.15	1.3128	46.735	339.0	1.0968	42.332	313.6
8	20	260.15	1.3084	50.131	255.8	1.3038	49.811	250.7
9	20	255.15	1.3778	50.174	173.1	1.3761	51.949	184.4
10	20	250.15	1.3899	50.162	125.2	1.3137	48.747	114.8
11	25	270.15	0.9441	34.756	349.3	0.8114	30.535	339.2
12	25	265.15	1.2911	48.904	319.4	1.3570	43.050	287.2
13	25	260.15	1.3705	50.268	226.6	1.3641	50.225	231.8
14	25	255.15	1.4093	50.126	154.0	0.8509	52.060	172.9
15	25	250.15	1.4085	50.239	106.4	1.3936	48.553	110.7
16	30	270.15	0.8595	34.574	297.6	1.3977	31.619	288.6
17	30	265.15	1.4058	50.133	247.2	0.8737	43.831	244.1
18	30	260.15	1.4017	50.103	185.1	1.4147	50.702	196.1
19	30	255.15	1.4052	50.153	120.6	0.8798	52.233	144.7
20	30	250.15	1.4065	50.11	80.4	1.4151	48.423	89.9
21	35	270.15	0.7139	27.129	214.2	1.1515	32.765	221.3
22	35	265.15	1.4195	50.201	184.4	1.4279	44.673	184.2
23	35	260.15	1.4114	50.162	136.7	1.1896	51.241	143.6
24	35	255.15	1.4125	50.161	85.8	1.4630	52.468	99.7

Table 5*:* Comparison of RSM and analysis results

Case	MVD	T_∞ (K)	Fluent Results			Regression Model		
			$c_{l,max}$	$(c_l/c_d)_{4^\circ}$	m_{ice}	$c_{l,max}$	$(c_l/c_d)_{4^\circ}$	m_{ice}
25	35	250.15	1.412	50.222	51.6	1.2109	48.354	52.3
26	40	270.15	0.6975	30.835	111.7	1.4135	33.973	137.3
27	40	265.15	1.4096	50.156	114.7	1.4815	45.577	107.6
28	40	260.15	1.4098	49.99	81.8	1.2156	51.841	74.5
29	40	255.15	1.4083	50.112	51.6	1.4168	52.765	38.0
30	40	250.15	1.4061	50.083	28.1	1.4833	48.347	-1.9
N1	37	260.23	1.4103	50.122	117.3	1.4147	51.412	118.6
N2	16.2089	254.513	1.3402	50.261	168.3	1.3254	51.825	172.6
N3	36.0137	259.244	1.4083	50.2	116.0	1.4378	51.965	123.5
N4	16.1668	257.946	1.2549	50.072	224.3	1.3006	51.239	222.6
N5	17.3978	260.872	1.1747	49.832	271.2	1.2478	48.847	263.8
N6	17.9864	262.055	1.2195	49.869	292.5	1.2144	47.396	279.1
N7	18.9743	262.338	1.2689	50.141	290.5	1.2167	47.091	281.2
N8	18.0822	262.873	1.2077	49.832	299.3	1.1826	46.195	289.8
N9	36.2707	258.634	1.4075	50.088	110.4	1.4507	52.300	115.3
N10	26.8379	268.125	0.5232	19.518	303.0	0.9816	36.593	303.0
N11	36.7181	267.742	1.3467	50.156	175.0	1.0567	39.524	178.1
N12	27.4361	253.18	1.4089	50.249	113.3	1.4377	51.334	138.6
N13	30.1414	268.423	0.4982	18.259	279.3	0.9839	36.469	272.0
N14	31.5207	269.845	0.7116	26.86	272.1	0.8841	32.853	267.5
N15	37.3635	262.445	1.4114	50.174	133.2	1.3412	49.231	130.5
N16	34.3102	265.172	1.404	50.198	193.6	1.2078	44.512	193.6
N17	31.9616	267.515	1.1457	48.046	247.2	1.0568	39.099	242.7
N18	38.1602	255.216	1.4144	50.256	65.4	1.4845	52.669	63.2
N19	16.8924	269.357	0.4088	11.088	375.8	0.7752	31.329	375.8
N20	20.4921	261.388	1.2698	50.297	272.5	1.2711	48.502	265.3

Table 6*:* Comparison of RSM and analysis results

CONCLUSION

This study aims to establish a model for the aerodynamic performance degradation of the NACA-22112 airfoil under in-flight icing conditions, specifically within the FAR-25 Appendix-C Continuous Maximum Envelope, based on ambient temperature and droplet diameter, while considering constant flight conditions. To achieve this objective, an adaptive sampling method is utilized for selecting icing condition samples, and a RSM is employed to generate a regression model that correlates the icing severity index with atmospheric conditions. For these purposes, the numerical methodology for ice accretion and aerodynamic performance calculation is initially validated using experimental data provided by Broeren et al. Subsequently, the validated methodology is employed in all simulations.

In order to assess aerodynamic performance loss due to icing, several criteria were considered, including ice mass on the airfoil, C_{Lmax}, and C_L/C_D at 4° AoA. These criteria were used to determine the icing severity index within the study. Correlation expressions between atmospheric variables and the given results were established using the response surface method. To efficiently utilize available resources and focus on the most sensitive points, the Design of Experiments strategy was implemented with an adaptive sampling method. This involved adding 20 new analysis points to the sample space, based on the results of 30 preliminary analyses conducted for the study.

The results indicate that ice accretion increases as the LWC value increases, leading to the transformation of the iced airfoil into a blunt structure, where glaze type icing occurs at ambient temperatures slightly below the freezing point. Although a blunt structure implies a higher decrease in aerodynamic efficiency, it becomes challenging to identify the exact point at which the critical loss begins. As a result, the regression model's mean error for the expanded sample increased for C_{Lmax} and C_L/C_D at 4° AoA but decreased for ice mass compared to the preliminary model. This is because the glaze ice cases in the new samples added to the analysis matrix disrupt the general trend in aerodynamic coefficients. However, for such problems, employing regression equation forms other than quadratic may yield more appropriate results. In summary, when the problem is segregated by icing types, the combined use of the RSM and adaptive sampling methods shows potential in achieving an overall correlation expression with a low error rate.

ACKNOWLEDGE

The authors are thankful for the computational resources of High-Performance Computing Center which provided by Turkish Aerospace.

References

Akbal, O., Ayan, E., Kaya, M.O., (2022) Atmosferik Koşullar Altında Uçak Kanat Profilinde Buz Birikim ve Performans Kestirimi, 9. Ulusal Havacılık ve Uzay Konferansı, UHUK-2022-094, September 2022.

Broeren, A.P., Addy, H.E. (2011) Aerodynamic Simulation of Ice Accretion on Airfoils, NASA Technical Paper, NASA/TP—2011-216929, June 2011.

Cebeci, T., and Besnard, E. (1994) Prediction of the Performance Degradation of Aircraft inNatural Icing Conditions, AIAA Paper 94-0487

Colaco, M.J., Dulikravich, G.S. (2011) A Survey of Basic Deterministic, Heuristic, and Hybrid Methods for Single Objective Optimization and Response Surface Generation, Thermal Measurements and Inverse Techniques, Vol. 1, p: 355-405, May 2011.

Fajt, N., Hann, R. and Lutz, T. (2019) The Influence of Meteorological Conditions on the Icing Performance Penalties on a UAV Airfoil, 8th European Conference for Aeronautics and Space Sciences (EUCASS), July 2019.

Gray, V. H. (1964) Prediction of Aerodynamic Penalties Caused by Ice Formations on Various Airfoils, NASA Technical Note, NASA TN D-2166, 1964.

Myers, R.H., Montgomery, D.C. (1995) Response Surface Methodology, Process and Product Optimization Using Designed Experiments, John Wiley & Sons, September 1995.

Phan, L. and Lin, C. (2019) CFD-based Response Surface Methodology for Rapid Thermal Simulation and Optimal Design of Data Centers, Advances in Building Energy Research, June 2019.

Regulations, FAA. (2013) Part 25-Airworthiness Standards: Transport Category Airplanes. Federal Aviation Administration (FAA), USA.

Shin, J., and Bond, T. H. (1992) Experimental and Computational Ice Shapes and Resulting Drag Increase for a NACA0012 Airfoil, NASA Glenn Research Center, January 1992.

Son, C., Yee, K., Oh, S. (2013) Numerical Correlation Between Meteorological Parameters and Aerodynamic Performance Degradation of Iced Airfoils, SAE 2013 Aerotech Congress & Exhibition, September 2013.

Zhang, M., Parnell, A., Brabazon, D., Benavoli, A. (2021) Bayesian Optimization for Sequential Experimental Design with Applications in Additive Manufacturing, arXiv:2107.12809v1, July 2021.

Zhang, Y., Neelakantan, A., Park, C., Kim, N.H., Lam, H., Haftka, R.T. (2019) Adaptive Sampling with Varying Sampling Cost for Design Space Exploration, American Institute of Aeronautics and Astronautics, Vol. 57, No. 3, March 2019.